

# A Unified Deep Learning Framework for Motion Correction in Medical Imaging

Jian Wang, Razieh Faghihpirayesh, Danny Joca, Polina Golland, Ali Gholipour, *Senior Member, IEEE*

**Abstract**—Deep learning has shown significant value in image registration, however, current techniques are either limited by the type and range of motion they can handle, or require iterative inference and/or retraining for new imaging data. To address these limitations, we introduce UniMo, a Unified Motion Correction framework that leverages deep neural networks to correct for diverse types of motion in medical imaging. UniMo exploits an alternating optimization scheme for a unified loss function to train an integrated model of 1) an equivariant neural network for global rigid motion correction and 2) an encoder-decoder network for local deformations. To this end, it features a geometric deformation augmenter that 1) enhances the robustness of global correction by addressing local deformations caused by non-rigid motion or geometric distortions, and 2) generates augmented data to improve the overall training process. UniMo is a hybrid model that uses both image intensities and shapes to achieve robust performance amid image appearance variations, and therefore generalizes effectively to multiple imaging modalities without requiring network retraining. We trained and tested UniMo to track motion in fetal magnetic resonance imaging, a particularly challenging application due to 1) the presence of both large rigid and non-rigid motion, and 2) wide variations in image appearance. We then evaluated the trained model, without retraining, on MedMNIST, lung CT, and BraTS datasets. The results show that UniMo surpassed existing motion correction methods in terms of accuracy, and notably enabled one-time training on a single modality while maintaining high stability and adaptability for inference across multiple unseen datasets. By offering a unified solution to motion correction, UniMo represents a significant advancement in medical imaging, especially in challenging applications with combined bulk motion and local deformations. The code is available at: <https://github.com/IntelligentImaging/UNIMO>

**Index Terms**—Deep Learning, Medical Image Registration, Motion Correction, Rigid Registration, Deformable Registration, Multi-Feature Fusion, Equivariant Neural Network

This work has been submitted to the IEEE for possible publication. Copyright may be transferred without notice, after which this version may no longer be accessible. This research was supported in part by the National Institutes of Health (NIH) under award numbers R01EB031849, R01EB032366, R01HD109395 and R01EB032708; in part by the Office of the Director of the NIH under award number S10OD025111, and in part by NVIDIA Corporation. The content of this publication is solely the responsibility of the authors and does not necessarily represent the official views of the NIH or NVIDIA.

Jian Wang was with Boston Children’s Hospital and Harvard Medical School, Boston, MA, USA (jianbljh@gmail.com).

Razieh Faghihpirayesh was with the Department of Electrical and Computer Engineering at Northeastern University and also with the Department of Radiology at Boston Children’s Hospital, Boston, MA, USA.

Danny Joca was with the Department of Radiology at Boston Children’s Hospital and Harvard Medical School, Boston, MA, USA.

Polina Golland is with the CSAIL (Computer Science and Artificial Intelligence Laboratory) at Massachusetts Institute of Technology (MIT), Cambridge, MA, USA.

Ali Gholipour is with the Department of Radiological Sciences and the Department of Electrical Engineering and Computer Science at the University of California Irvine, CA, USA (ali.gholipour@uci.edu).

Manuscript received September 2025.

## I. INTRODUCTION

Motion remains to be a challenge in medical imaging. For reliable imaging and image analysis, motion should be avoided, corrected, or compensated for, for reliable image analysis [1]–[4]. Although classical image registration methods can be effective for motion correction, they often necessitate full execution of an optimization process on non-convex cost functions that only act as a surrogate measure of image alignment [5]–[9]. Thus, these techniques are typically limited by a narrow capture range, especially when addressing large motions. This constraint reduces their precision and applicability in challenging applications such as fetal MRI where subjects may move in wide angles [10]–[12]. To address these limitations, recent research has increasingly turned to deep learning based models for motion estimation/correction [13].

Deep learning-based motion correction techniques have seen widespread applications across various imaging modalities, with significant developments in two main areas: i) A major focus on Magnetic Resonance Imaging (MRI), including functional MRI (fMRI), T1-, T2-, and diffusion-weighted MRI, and quantitative MRI. These models are extensively studied due to their broad applicability and substantial impact in the field, covering a wide range of clinical scenarios. ii) Motion correction for other modalities, such as ultrasound, positron emission tomography (PET), and Computed Tomography (CT) where advancements and methodologies are also being explored.

Learning-based motion correction in MRI focuses on two key approaches: i) image-based motion correction and ii) techniques using k-space data. Image-based methods target motion correction by processing reconstructed MRI images with deep neural networks, such as Convolutional Neural Networks (CNNs) [11], [14] and other deep learning architectures [15]–[18]. These approaches often employ convolutional encoder-decoder networks, leveraging downsampling and upsampling for feature extraction and reconstruction [19], [20]. Advanced models like U-Nets, recurrent neural networks, and transformers have been proposed to handle temporal dependencies and spatial relationships [15], [18], [21]–[23]. Additionally, prior-assisted methods improve correction by incorporating supplementary data such as multi-contrast or dynamic images, enhancing performance through architectures that integrate this information [24], [25]. These methods offer robust solutions by combining motion correction with other learning-based tasks, ultimately improving MRI reconstruction quality, e.g. [23].

K-space-based motion correction methods, on the other hand, leverage raw k-space data with MR reconstruction to mitigate motion artifacts through deep learning techniques. These include deep neural networks for noise-resilient motion

correction and motion parameter estimation [26]–[28], and methods that combine motion detection with traditional reconstruction [29]. One approach targets artifacts by detecting motion directly from k-space images and data using CNNs [30], while others use temporal information [31] or end-to-end motion models to enhance reconstruction quality and reduce acquisition times [32]. Additionally, generative models and implicit neural representations (INRs) offer subject-specific solutions to handle unique motion characteristics [33], [34].

In the domain of ultrasound and PET imaging also, significant advancements in motion correction have been achieved. For instance, approaches [35] that combine affine and nonrigid motion estimation have proven effective in addressing both large-scale and fine deformations, leading to improved image quality. The use of CNNs for 3D freehand ultrasound reconstruction has streamlined the motion estimation process [36], bypassing traditional physical models, while resulting in more accurate and reliable ultrasound imaging. Motion correction techniques based on PET utilizing bidirectional 3D long short-term memory networks have been effective in addressing inter-frame rigid motion in dynamic cardiac PET, improving both motion estimation and myocardial blood flow quantification [37]. Similarly, deep learning models designed to predict rigid motion parameters directly from PET data have shown promise in correcting head motion in brain PET scans [38].

Despite significant advancements, state-of-the-art methods remain heavily constrained by the specific imaging datasets and modalities they are trained on and the types of motion they can handle, which limit their effectiveness in correcting motion in unseen imaging domains. While one approach [17] shows promise in handling motion for unseen modalities, it struggles with large motions in image pairs that are heavily contaminated by noise [39] and those that exhibit contrast changes. For instance, substantial intensity and contrast variations in images pose significant challenges, as current algorithms largely rely on image intensities while overlooking shape information. This limits generalization capacity of the trained models.

On the other hand, continuous advances in deep learning have enabled reliable and accurate segmentation and landmark detection, supporting their effective use in image registration. Compared to traditional intensity-based methods, shape- and keypoint-based approaches [14], [40]–[42] now provide robust alternatives, particularly in challenging imaging scenarios. Building on these developments, our joint optimization framework integrates shape cues to improve registration performance. This reflects a broader shift in the field toward leveraging geometric representations derived from learned features, which have demonstrated strong generalization across datasets and modalities [40]. Motivated by the need for generalizable and accurate motion correction across diverse imaging conditions, we introduce UniMo—a unified method that combines shape and intensity information to correct both bulk rigid motion and local deformations. UniMo capitalizes on the strengths of deep learning while avoiding the need for extensive retraining. Therefore, it offers a robust and efficient solution that is adaptable to various imaging conditions. By not imposing restrictive assumptions about motion types or ranges, UniMo ensures stable and accurate correction for a range of

applications. Moreover, eliminating the retraining requirement reduces computational overhead and enables seamless integration into imaging workflows, which advances the state of the art in motion estimation and correction.

The main contributions of this work (UniMo) are:

- UniMo is the first method for generalizable correction of both rigid and non-rigid motion without a need for retraining in a new domain.
- UniMo offers motion correction of a pair of images with stable convergence in training and real-time inference.
- UniMo capitalizes on the synergies between global rigid motion estimation and local deformation correction. This innovative strategy demonstrates its versatility through its broad applicability to various joint learning tasks.

## II. BACKGROUND

In this section, we review the theories of rigid motion correction, deformable image registration, and joint optimization.

### A. Rigid Motion Estimation via Equivariant Filters

Rigid motion estimation aims to identify the best translation  $\mathcal{T}$  and rotation  $\mathcal{R}$  parameters that define a rigid transformation  $Q(\mathcal{T}, \mathcal{R})$  between a pair of images. In a simple form, this process may be formulated as minimizing the Euclidean distance  $d$  between a source image  $S$  and a target image  $T$ ,

$$E[Q(\mathcal{T}, \mathcal{R})] = \text{Dist}[S \circ Q(\mathcal{T}, \mathcal{R}), T] + \text{Reg}(\mathcal{T}, \mathcal{R}), \quad (1)$$

where  $\circ$  is the composition operator that resamples  $S$  using the rigid transformation  $Q(\mathcal{T}, \mathcal{R})$ . When this operator is applied to any vector  $\mathbf{v}$ , it yields a transformed vector  $Q(\mathbf{v})$  of the form  $Q(\mathbf{v}) = \mathcal{R}\mathbf{v} + \mathcal{T}$ . Here,  $\mathcal{R}^T = \mathcal{R}^{-1}$  indicating that  $\mathcal{R}$  is an orthogonal matrix.

Rather than estimating the transformation function  $Q$  directly in the original image space, efficient approaches have demonstrated that it can be computed using low-dimensional representations, such as key points or equivariant features of images [17]. In specific, equivariant filters have shown proven stability and accuracy in rigid image registration. The closed-form solution for both translation and rotation parameters is:

$$\mathcal{T} = \bar{T} - \mathcal{R}\bar{S}, \quad \mathcal{R} = V \cdot U^T, \quad \text{s.t. } \det(\mathcal{R}) = 1, \quad (2)$$

where  $\bar{S}$ ,  $\bar{T}$  represent the low-dimensional representations of the source and target images respectively.  $U\Sigma V^* = \bar{S} \cdot \bar{T}^T$ ,  $U$  and  $V^*$  are real orthogonal matrices,  $\Sigma$  is a diagonal matrix with non-negative real numbers on the diagonal. The condition on the determinant of  $\mathcal{R}$  in Eq. (2) is set to ensure it accurately reflects a rigid rotation.

### B. Deformation Correction via Deformable Registration

In addition to global rigid transformations, deformations may be needed to align medical images to compensate for elasticity of tissue/organs, anatomical variations (between subjects or across time), or geometric distortions as imaging artifacts. In this section, we provide an overview of the Large Deformation Diffeomorphic Metric Mapping (LDDMM) algorithm for image registration [43] between the rigid motion-corrected

image  $S \circ Q(\mathcal{T}, \mathcal{R})$  and the target image  $T$ . For simplicity, we denote  $S \circ Q(\mathcal{T}, \mathcal{R})$  as  $\hat{S}$ .

Let  $\hat{S}$  be a source image and  $T$  be a target image defined on a torus domain  $\Gamma = \mathbb{R}^d / \mathbb{Z}^d$  ( $\hat{S}(x), T(x) : \Gamma \rightarrow \mathbb{R}$ ). The problem of diffeomorphic image registration is to find the shortest path to generate time-varying diffeomorphisms  $\{\psi_t\} : t \in [0, 1]$  such that  $\hat{S} \circ \psi_1$  is similar to  $T$ , where  $\circ$  is a composition operator that resamples  $\hat{S}$  by the smooth mapping  $\psi_1$ . This is typically solved by minimizing the energy function of LDDMM [43] over an initial velocity field  $v_0$ .

For computational efficiency, we employ a fast version of LDDMM that characterizes deformations as  $\{\psi_t\}$  in a low-dimensional band limited space. The corresponding time-dependent tangent vector of such deformations can be determined by an initial condition  $\tilde{v}_0$ ,

$$E(\tilde{v}_0) = \text{Dist}(\hat{S} \circ \psi_1, T) + (\tilde{\mathcal{L}}\tilde{v}_0, \tilde{v}_0), \quad (3)$$

where the distance function  $\text{Dist}(\cdot, \cdot)$  measures the dissimilarity between images. Commonly used distance functions include sum-of-squared difference of image intensities [43], normalized cross correlation [44], and mutual information [41], [45]. The regularization term  $(\tilde{\mathcal{L}}\tilde{v}_0, \tilde{v}_0)$  enforces spatial smoothness of transformations with  $\tilde{\mathcal{L}}$  being a symmetric and positive-definite differential operator in the Fourier domain. It converts a vector field  $\tilde{v}$  to a momentum vector by  $\tilde{m} = \tilde{\mathcal{L}}\tilde{v}$ . The deformation  $\psi_1$  corresponds to  $\tilde{\psi}_1$  in Fourier space via the Fourier transform  $\mathcal{F}(\psi_1) = \tilde{\psi}_1$ , or its inverse  $\psi_1 = \mathcal{F}^{-1}(\tilde{\psi}_1)$ .

Let  $\widetilde{\text{Diff}}(\Omega)$  and  $\tilde{V}$  denote the bandlimited space of diffeomorphisms and velocity fields respectively. The Euler-Poincaré differential (EPDiff) equation [46], [47] is reformulated in a complex-valued Fourier space with much less dimensions, i.e.,

$$\frac{\partial \tilde{v}_t}{\partial t} = -\tilde{\mathcal{K}} \left[ (\tilde{\mathcal{D}}\tilde{v}_t)^T \star \tilde{\mathcal{L}}\tilde{v}_t + \tilde{\nabla} \cdot (\tilde{\mathcal{L}}\tilde{v}_t \otimes \tilde{v}_t) \right], \quad (4)$$

where  $\star$  is a circular matrix-vector field auto-correlation<sup>1</sup>.  $\tilde{\mathcal{K}}$  is a smoothing operator and  $\tilde{\mathcal{D}}\tilde{v}$  is a tensor product with  $\tilde{\mathcal{D}}(\xi) = i \sin(2\pi\xi)$  representing the Fourier frequencies of a central difference Jacobian matrix  $D$ . The operator  $\tilde{\nabla} \cdot$  is the discrete divergence operator that is computed as the sum of the Fourier coefficients of the central difference operator  $\tilde{D}$  along each dimension, i.e.,  $\tilde{\nabla} \cdot \xi = \sum_{j=1}^d i \sin(2\pi\xi_j)$ . Since  $\tilde{\mathcal{K}}$  on the left side of Eq. (4) is a low-pass filter that suppresses high frequencies in the Fourier domain, all operations are easy to implement in a truncated low-dimensional space by eliminating high frequencies.

The diffeomorphic transformations can also be represented in the frequency domain [48] as  $\tilde{\psi}_t$ ,

$$\frac{d\tilde{\psi}_t}{dt} = -\tilde{\mathcal{D}}\tilde{\psi}_t * \tilde{v}_t, \quad (5)$$

where  $*$  is a circular convolution.

<sup>1</sup>Auto-correlation operates on zero-padded signals followed by truncating to the bandlimits in each dimension to ensure the output remains bandlimited.

### C. Joint Optimization

A joint optimization approach estimates both rigid transformation  $Q(\mathcal{T}, \mathcal{R})$  and deformation  $\tilde{v}_0$  by integrating a combination of Eq. (1) and Eq. (3),

$$\begin{aligned} E[Q(\mathcal{T}, \mathcal{R}), \tilde{v}_0] &= E[Q(\mathcal{T}, \mathcal{R})] + E(\tilde{v}_0) \\ &= \underbrace{\text{Dist}[S \circ Q(\mathcal{T}, \mathcal{R}), T] + \text{Reg}(\mathcal{T}, \mathcal{R})}_{\text{Rigid Motion Correction}} \\ &\quad + \underbrace{\text{Dist}(\hat{S} \circ \psi_1(\tilde{v}_0), T) + (\tilde{\mathcal{L}}\tilde{v}_0, \tilde{v}_0)}_{\text{Deformation Correction}}, \\ &\quad \text{s.t. Eq. (2), Eq. (4) \& Eq. (5)} \quad (6) \\ &\quad \text{Joint Constraints} \end{aligned}$$

Such joint approaches have demonstrated enhanced accuracy and robustness for single image modalities [15], [16]. However, these frameworks fall short when image pairs exhibit significant intensity changes. The issue arises because both dissimilarity terms in Eq.(6) are highly dependent on the images themselves, increasing the likelihood that the optimization will be biased by intensity variations. This limitation motivated the development of a hybrid motion correction framework that integrates knowledge from both image intensities and shape to effectively reduce errors caused by image intensity variations.

## III. METHODOLOGY

### A. Hybrid Motion Correction

In this section, we present a hybrid motion correction approach that utilizes both image and shape information. Our objective is to develop an optimal motion correction solution, denoted as  $Q(\mathcal{T}, \mathcal{R})$ , which exhibits increased robustness to variations in image intensity. We first define the basic composition operation between two rigid transformations,

$$Q(\mathcal{T}, \mathcal{R}) = [(1 - \lambda) \cdot Q_I(\mathcal{T}_I, \mathcal{R}_I)] \odot [\lambda \cdot Q_G(\mathcal{T}_G, \mathcal{R}_G)], \quad (7)$$

where  $\lambda$  denotes the weight parameter balancing the effect of both domains, and  $\odot$  is a spherical linear interpolation operator. Here,  $Q_I$  and  $Q_G$  denote the rigid transformations estimated from images and segmentations separately. In this work, we apply distance transform to segmentation maps to represent the most straightforward geometric shape of images. Other intensity-invariant shape descriptors [49], [50] can be easily integrated into our framework as well.

After obtaining the hybrid rigid transformation  $Q$ , for deformation estimation we estimate  $\tilde{v}_0^I$  and  $\tilde{v}_0^G$  (representing the transformation fields) in the spatial domain for images and segmentations respectively. The derivation of a hybrid velocity field is not the primary objective of this work. Instead, we formalize the hybrid objective function for optimization as follows,

$$E[Q, \tilde{v}_0^I, \tilde{v}_0^G] = E[Q(\mathcal{T}, \mathcal{R})] + E(\tilde{v}_0^I) + E(\tilde{v}_0^G). \quad (8)$$

### B. Hybrid Rigid Transformation for Motion Correction

In this section, we show the derivations of computing  $Q$  step by step. To maintain the properties of  $SO(3)$  generated by estimated rigid transformations, we employ spherical linear interpolation instead of simple linear addition. Such interpolation

enables smooth and consistent interpolation between rotations by following the shortest path, or geodesic, on the unit sphere. Our approach ensures that the interpolated rotation remains within the  $SO(3)$  manifold, preserving the orthogonality and unit length essential for valid rotations. We avoid the pitfalls of directly adding rotation matrices or quaternions, thereby ensuring that the combined rotation is both mathematically correct and physically meaningful. This preservation of the rotational manifold's integrity is crucial in applications such as computer graphics, robotics, and medical imaging, where accurate and reliable rotational transformations are required [51]–[53].

We derive  $\mathbf{Q}$  by computing two rigid transformation matrices,

$$\mathcal{Q}_I = \begin{bmatrix} \mathcal{R}_I & \mathbf{t}_I \\ \mathbf{0}^T & 1 \end{bmatrix}, \quad \mathcal{Q}_G = \begin{bmatrix} \mathcal{R}_G & \mathbf{t}_G \\ \mathbf{0}^T & 1 \end{bmatrix},$$

- 1) Convert  $\mathcal{R}_I$  and  $\mathcal{R}_G$  to quaternions  $\mathbf{q}_I$  and  $\mathbf{q}_G$ ;
- 2) Apply spherical linear interpolation to  $\mathbf{q}_I$  and  $\mathbf{q}_G$  with weight  $\lambda$  and a calculated angle  $\theta$  in Appendix A,

$$\mathbf{q} = \frac{\sin((1-\lambda)\theta)}{\sin(\theta)} \cdot \mathbf{q}_I + \frac{\sin(\lambda\theta)}{\sin(\theta)} \cdot \mathbf{q}_G;$$

- 3) Convert  $\mathbf{q}$  back to a rotation matrix  $\mathcal{R}$  (details in Appendix A);
- 4) Linearly combine translations,

$$\mathcal{T} = (1-\lambda)\mathcal{T}_I + \lambda\mathcal{T}_G;$$

- 5) The final hybrid rigid transformation matrix is

$$\mathbf{Q} = \begin{bmatrix} \mathcal{R} & \mathcal{T} \\ \mathbf{0}^T & 1 \end{bmatrix}$$

We also set  $\det(\mathcal{R}) = 1$ . Our strategy ensures that the resulting transformation maximally preserves  $SO(3)$  properties.

### C. Network Design and Training

We develop a deep learning framework to estimate the objective expressed in Eq. (8). Our framework comprises two major sub-modules: i) A hybrid rigid motion correction neural network, parameterized by equivariant filters, to produce  $\mathbf{Q}$ ; and ii) A hybrid deformation correction network, implemented using UNet, with deformable shape augmentation to estimate  $\tilde{v}_0^I$  and  $\tilde{v}_0^G$ . Our framework is illustrated in Fig. 1. In the following sections, we provide a detailed description of the network architecture and the formulation of the network loss.

**Hybrid Rigid Motion Correction Equivariant Network:** Let  $\Theta = (\mathcal{T}_I, \mathcal{R}_I, \mathcal{T}_G, \mathcal{R}_G)$  represent the encoder parameters that learn rigid parameters from image and shape spaces, with  $Q_I(\Theta)$  and  $Q_G(\Theta)$  denoting the transformation functions yielded by the learned rigid parameters from the low-dimensional representations. Let  $\mathbf{Q}$  denote the hybrid rigid transformation. The rigid correction loss is computed between the aligned outputs and targets. Note that CNNs or recurrent neural networks can also be used for extracting low-dimensional features from images [11], [14], [21]. However, such representations are limited in capturing the true nature of rigid transformations. In our approach, we employ an efficient method to compute rigid transformations within the

equivariant neural network by calculating the spatial means of images [17]. We express the general formulation for the rigid motion network, which takes source images (or segmentations) and target images (or segmentations), as follows:

$$l(\Theta) = \|S \circ \mathbf{Q}(\Theta) - T\|_F, \quad \text{s.t. Eq. (2) \& Eq. (7),} \quad (9)$$

where  $\|\cdot\|_F$  denotes the Frobenius norm.

**Deformation Correction Network:** Let  $\Phi$  denote the parameters of an encoder-decoder in our geometric learning network, where  $\psi_I(\Phi)$  represents the deformation fields and  $\tilde{v}_0(\Phi)$  represents the velocity fields learned by the network. The general formulation of the loss for the deformation estimation network, which takes aligned images (or segmentations) and target images (or segmentations), is given by:

$$\begin{aligned} l(\Phi) = & \frac{1}{\sigma^2} \|S \circ \mathbf{Q}(\Theta) \circ \psi(\Phi) - T\|_2^2 + (\tilde{\mathcal{L}}\tilde{v}_0(\Phi), \tilde{v}_0(\Phi)) \\ & + \text{reg}(\Theta, \Phi), \quad \text{s.t. Eq. (4) \& Eq. (5).} \end{aligned} \quad (10)$$

In addition to estimating deformations using LDDMM [48], we provide a deep learning model that learns stationary velocity fields [54] while maintaining comparable model accuracy. Advanced predictive image registration models, including TransMorph [55] and DiffuseMorph [56], can be integrated into our framework. Analogous to our previous work [15], we extend UniMo to a spatio-temporal approach that incorporates time information to handle motion among data sequences.

**Network Loss.:** The objective function for the hybrid model is defined as:

$$l(\Phi, \Theta) = l_I(\Phi) + l_G(\Phi) + l_I(\Theta) + l_G(\Theta). \quad (11)$$

We employ an alternating optimization scheme [57] to minimize the network loss.

## IV. EXPERIMENTAL EVALUATION

**Data:** For motion correction and tracking in a single domain (modality) test, we included 240 sequences of 4D fetal echo-planar imaging (EPI) time series acquired on Siemens 3T scanners. The study was approved by the institutional review board and written informed consent was obtained from all participants. The gestational ages of the fetuses at the time of the scans were from 22.57 to 38.14 weeks (mean 32.39 weeks). Imaging parameters included a slice thickness of 2 to 3mm, a repetition time of 2 to 5.6s (mean 3.1s), and an echo time of 0.03 to 0.08s (mean 0.04s). Fetal brains were extracted from scans using a previously-validated segmentation method [58]. All brain scans were resampled to  $96^3$  with a voxel size of 3mm $^3$  and underwent intensity normalization.

For multiple, out-of-domain modality tests, in all baselines, we incorporated three different image datasets, including segmentation labels from varying organs, CT scans, and T1 MRIs, from publicly released medical image repositories. We used 60 CT scans from the Lung CT Segmentation Challenge (LCTSC) [59]. This dataset comprises 4DCT or free-breathing CT images (slice thickness of 2.5 to 3 mm) from 60 patients across three institutions, divided into 36 training datasets, 12 off-site test datasets, and 12 live test datasets. Manual segmentations are provided and serve as the ground truth,

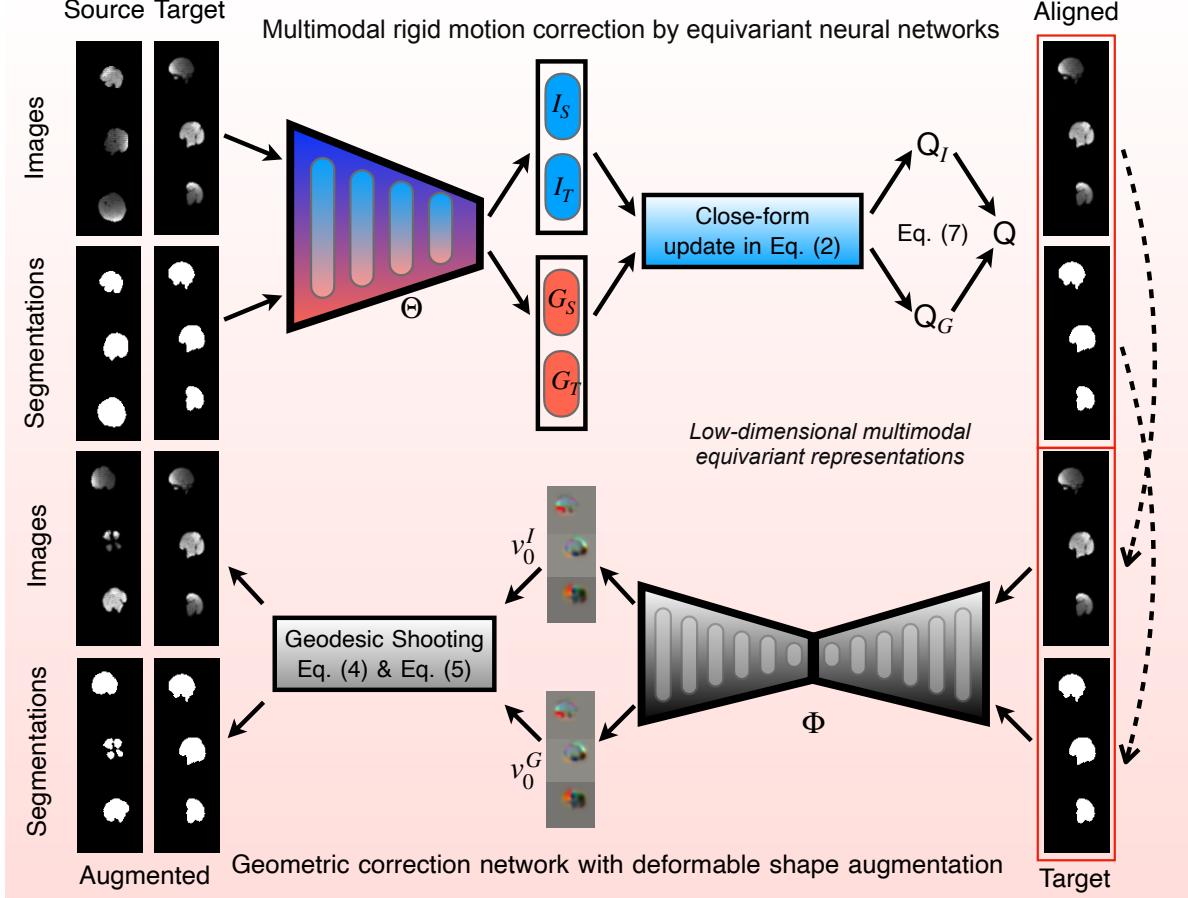


Fig. 1. An illustration of the network architecture of our proposed motion correction learning framework, UniMO. **Top:** Motion correction is based on equivariant neural networks that take both images and segmentations as input. The low-dimensional spatial means of the images and segmentations are estimated simultaneously. An enhanced hybrid rigid transformation  $Q$  is computed from both domains. The rigid loss function is calculated between the aligned and target images/labels. **Bottom:** A geometric shape augmenter is incorporated into the U-Net based neural networks. It takes both aligned and target images/segmentations and estimates the transformation fields for both domains using separate loss functions for segmentations and images.

including the esophagus, heart, lungs, and spinal cord. For our work, we specifically extracted the left and right lungs for registration. Second, we included 200 images (slice thickness of  $1 \text{ mm}^3$ ) from the MedMNIST datasets of varying organs [60], [61]. The scans consisted of 3D CT scans of the adrenal gland, 3D CT scans of bone fractures, and 3D magnetic resonance angiography (MRA) scans of blood vessel shapes in the brain, as manually-segmented labels. We applied Gaussian smoothing filter to pre-process all binary maps. Third, for 3D brain tumor MRI scans with tumor segmentation labels, we included 200 public T1-weighted brain scans of different subjects from Brain Tumor Segmentation (BraTS) [62], [63] challenge 2021. All volumes from these datasets were resampled to  $96^3$ , with a voxel resolution of  $1 \text{ mm}^3$ , and underwent intensity normalization and bias field correction.

**Motion Simulation:** Simulations for synthetic motion on real training and test data were performed on preprocessed, intensity-normalized image volumes. Rigid motion was modeled as six-degree-of-freedom transformations (translations in millimeters, rotations in degrees) applied about the image centroid. Non-rigid motion was modeled as B-spline free-

form deformations on voxel grids with bounded control-point perturbations. Non-rigid fields were composed with rigid transforms, and images were resampled using linear interpolation.

Rigid motion was generated in two ways: 1) by interpolating a source-target transformation into 10 steps and 2) by random-walk trajectories with Gaussian increments ( $\sigma_T = 0.5\text{--}2.0 \text{ mm}$ ,  $\sigma_R = 0.2\text{--}1.0^\circ$ ) smoothed temporally by splines. Two regimens were used: small motion (translations  $\leq 10 \text{ mm}$ , rotations  $\leq 5^\circ$ ) and large motion (translations  $\leq 30 \text{ mm}$ , rotations  $\leq 20^\circ$ ). For fetal EPI, non-rigid fields were generated on B-spline grids with control point spacing of 8–12 voxels (corresponding to 24–36 mm at 3 mm resolution) and perturbations  $\leq 3 \text{ mm}$ . For lung CT, non-rigid fields were generated on grids with spacing of 10 voxels (10 mm at 1 mm resolution) and perturbations of 3–5 mm, with diaphragm regions allowing up to 7–10 mm to mimic respiratory deformation. For structural MRI, non-rigid fields were generated on grids with spacing of 10 voxels (10 mm at 1 mm resolution) and perturbations  $\leq 3 \text{ mm}$ . Ground-truth frame-wise rigid transformations and non-rigid fields were recorded for quantitative evaluation of translational, angular, and overlap-based metrics.

**Baselines & Evaluation Metrics.**: We conducted three sets of experiments to evaluate UniMo: i) an ablation study of the most important weight parameter that balances the effect between shape and image, ii) motion correction performance on single image modality (fetal EPI), and iii) motion correction on the out-of-domain image modalities (LCTSC, MedMNIST, and BraTS) without network retraining.

First, we examined the estimated values of the weight parameter  $\lambda$  with different initial values as convergence curves during network training. Next, we compared our model against state-of-the-art deep learning motion correction approaches, including DeepPose [11], KeyMorph [14], and Equivariant Filters [17]. Our evaluation includes both visual comparisons and quantitative analyses, focusing on translational and angular errors in data with simulated motions. Additionally, we use a voxel-wise metric, temporal Signal to Noise Ratio (tSNR), to assess the quality and alignment of the EPI time series in the single modality task. Misalignment or motion degradation across an image time series lowers tSNR.

To test the sub-module of our spatial-temporal approach for 4D EPI motion tracking, we treated all baselines as static models to predict motion parameters between subsequent images of the time series. For both motion correction and tracking, we tested all models on real EPI scans with unknown motions, reporting the Dice coefficient between the target image and the aligned image. The effectiveness and stability of motion correction are demonstrated through a Dice coefficient analysis, comparing the alignment accuracy of images across different degrees of motion and sequence lengths.

To evaluate the effectiveness of UniMo compared to baselines trained on multiple image modalities, we first report the translational and angular errors on simulated motions for all models. We present multiple examples, comparing all models across different image modalities. To demonstrate the advantage of UniMo, which does not require retraining with limited datasets, we also report mean Dice accuracy and the best epoch number for model training, including the deviation as the size of the training dataset increases.

**Implementation & Parameters:** For motion correction settings, we set the dimension of low-dimensional key points to 128 when computing the close-form update of rigid transformation. We included a nine-layer equivariant neural network with two attention layers. For the geometric shape augmenter, we adopted a 7-layer Unet and used 16 as the reduced dimensionality of the low-dimensional frequencies in Eq. (4). We used 10 time steps of Euler integration for geodesic shooting. We adopted an automated method for updating the weight parameter  $\lambda$  by treating it as a network parameter. For network training, we used a batch size of 4, a weight decay of 0.00001 for  $L_2$  regularization, and an initial learning rate of  $\eta = 1 \times 10^{-5}$ , with training conducted for 1000 epochs using the Adam optimizer. The learning rate schedule employed cosine annealing to dynamically adjust the rate throughout training. The dataset was divided into 70% for training, 15% for validation, and 15% for testing. The best-performing models were selected based on validation performance. All experiments were carried out on an NVIDIA RTX A6000 GPU with 48GB memory.

## V. RESULTS

### A. Single Modality Evaluation

Fig. 2 visualizes two cases of tSNR heat maps calculated over 50 pairs for motion correction across all models. The heat maps demonstrate that UniMo displays higher tSNR values than other methods, indicating that UniMo accurately corrected motions and produced aligned images with higher accuracy than the alternative methods.

The left side of Fig. 3 presents a comparative analysis of motion correction errors in translation and rotation across all methods. Our approach produced the lowest errors ( $\sim 2.4$  mm of movement, and  $\sim 1.8^\circ$  of rotations for the fetal brain) with lowest variance between adjacent 3D volumes compared to other methods. It highlights the superior performance of UniMo in correcting fetal motions, consistently surpassing the state-of-the-art methods in accuracy.

The right side of Fig. 3 illustrates a comparison of motion tracking errors in translation and rotation across various methods. Our method achieves the lowest error rates for 70 image sequences, with approximately 4.8 mm for translational movements and 2.3 degrees for rotational adjustments in fetal brain scans. UniMo exhibits lower alignment error between consecutive 3D volumes compared to the alternative methods, reflecting its superior motion tracking accuracy. Note that in this scenario on motion tracking on a 3D image time series, static models produced higher errors because they were not able to capture the long-term image sequence dependencies.

The right side of Fig. 4 quantitatively shows the accuracy of motion tracking comparison over varying degrees of motions and different lengths of data sequences. Our model exhibits superiority in handling real motions ranging from small to large, and it maintains comparable motion tracking accuracy when dealing with extended data sequences. This indicates the high stability and robustness of our model, as it demonstrates a high level of accuracy in correcting severe fetal brain movements. We also report the average time consumption for adjacent pairs and the entire sequence. The total computation time of our model for motion tracking is 10 seconds for a 4D sequence that takes  $\sim 60$ s to acquire. This paves the way for an efficient real-time tracking of the fetal head motion for prospective correction.

The left side of Fig. 4 shows the dice coefficient comparisons for fetal EPI image pairs under various motion levels. It demonstrates that our method consistently achieves higher dice scores, regardless of the motion degree. This highlights the robustness and stability of our model, particularly in challenging scenarios with significant motion occurrences.

### B. Cross-modality Evaluation

Fig 5 shows eight cases of motion correction comparisons across multiple modalities, including T1 MRI, fetal EPI scans, lung CT scans, and organ shapes from MedMNIST. Our method, trained on a single modality, consistently outperforms all methods trained on multiple modalities. Specifically, for T1 MRI, fetal EPI scans, and organ shapes from MedMNIST, our method significantly outperforms KeyMorph and DeepPose and slightly surpassed the equivariant filter model. For

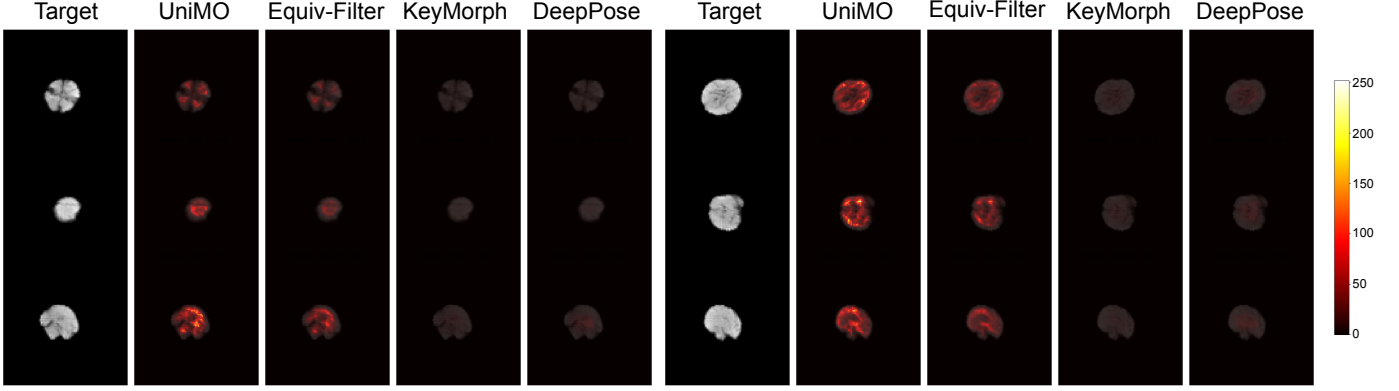


Fig. 2. Two examples of heat maps of tSNR estimated from all motion correction models over 50 fetal EPI pairs. From left to right: Target image, heat maps from UniMO, Equiv-Filter, KeyMorph and DeepPose. Higher tSNR values indicate the best alignment of the image time series was obtained from UniMo.

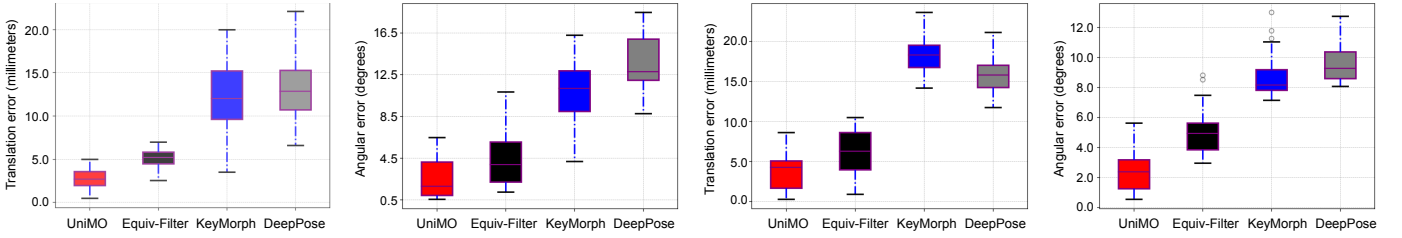


Fig. 3. Statistical results for both transnational and angular errors of all models on single modality. Left: motion correction performance reported over 300 image pairs; Right: motion tracking performance on 70 sequences of fetal EPI scans with simulated motions.

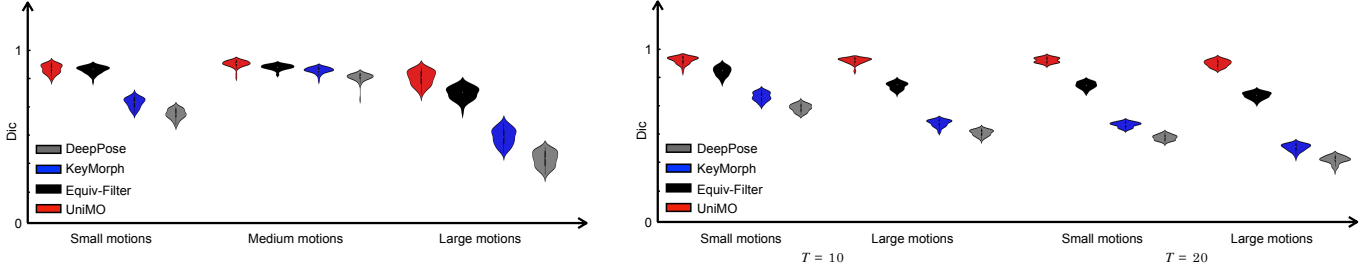


Fig. 4. Statistical results of Dice comparison on fetal EPIs with unknown motions. Left: Motion correction performance with different degrees of motions, small ( $T_{max} = 10\text{mm}$ ,  $\mathcal{R}_{max} = 5^\circ$ ), medium ( $T_{max} = 20\text{mm}$ ,  $\mathcal{R}_{max} = 10^\circ$ ) and large motions ( $T_{max} = 30\text{mm}$ ,  $\mathcal{R}_{max} = 20^\circ$ ). The dice score of our best model, for motion levels from left to right are, 0.97, 0.93, 0.92. Right: motion tracking performance across varying degrees and lengths of image sequences ( $T$ ). Small ( $T_{max} = 10\text{mm}$ ,  $\mathcal{R}_{max} = 5^\circ$ ) and large motions ( $T_{max} = 30\text{mm}$ ,  $\mathcal{R}_{max} = 20^\circ$ ) were evaluated. Report efficiency with average time consumption: **0.501s** per pair / **9.960s** per sequence when  $T = 20$ .

lung CT scans, where image intensities exhibited significant contrast variations, our model, UniMO, demonstrated superior performance compared to all other baselines. This is because other models tend to neglect shape information when estimating motion parameters, focusing predominantly on image intensities. In contrast, UniMO effectively integrates shape information, leading to more accurate motion correction. The visualization demonstrates that our model can be effectively employed across various modalities with high accuracy.

The left side of Fig. 6 presents the statistical comparison of motion correction across all models. UniMO demonstrates the lowest error, with an average error of 2.51 mm and a rotation of about 1.9 degrees, across various image modalities. These results partially highlight the benefits of incorporating shape information that allowed UniMo achieve high performance across different image modalities, whereas the other

techniques performed poorly. The right side of Fig. 6 illustrates the optimal epoch of model training and Dice accuracy for various training dataset sizes. Our model demonstrates rapid convergence and maintains consistently high accuracy even with datasets smaller than 50 samples. In contrast, baseline models such as KeyMorph and DeepPose show gradual improvements in accuracy as the training dataset size increases. This is attributed to their limited capability to accurately learn and generalize the nature of rigid motion across different image modalities. Although the original equivariant filter model performs relatively well when the dataset size is reduced to one third, its average accuracy is still compromised in cases where image intensities exhibit significant variations. Our method, however, effectively captures the inherent characteristics of rigid transformations and remains robust against fluctuations in image intensities and contrast. This highlights the superior

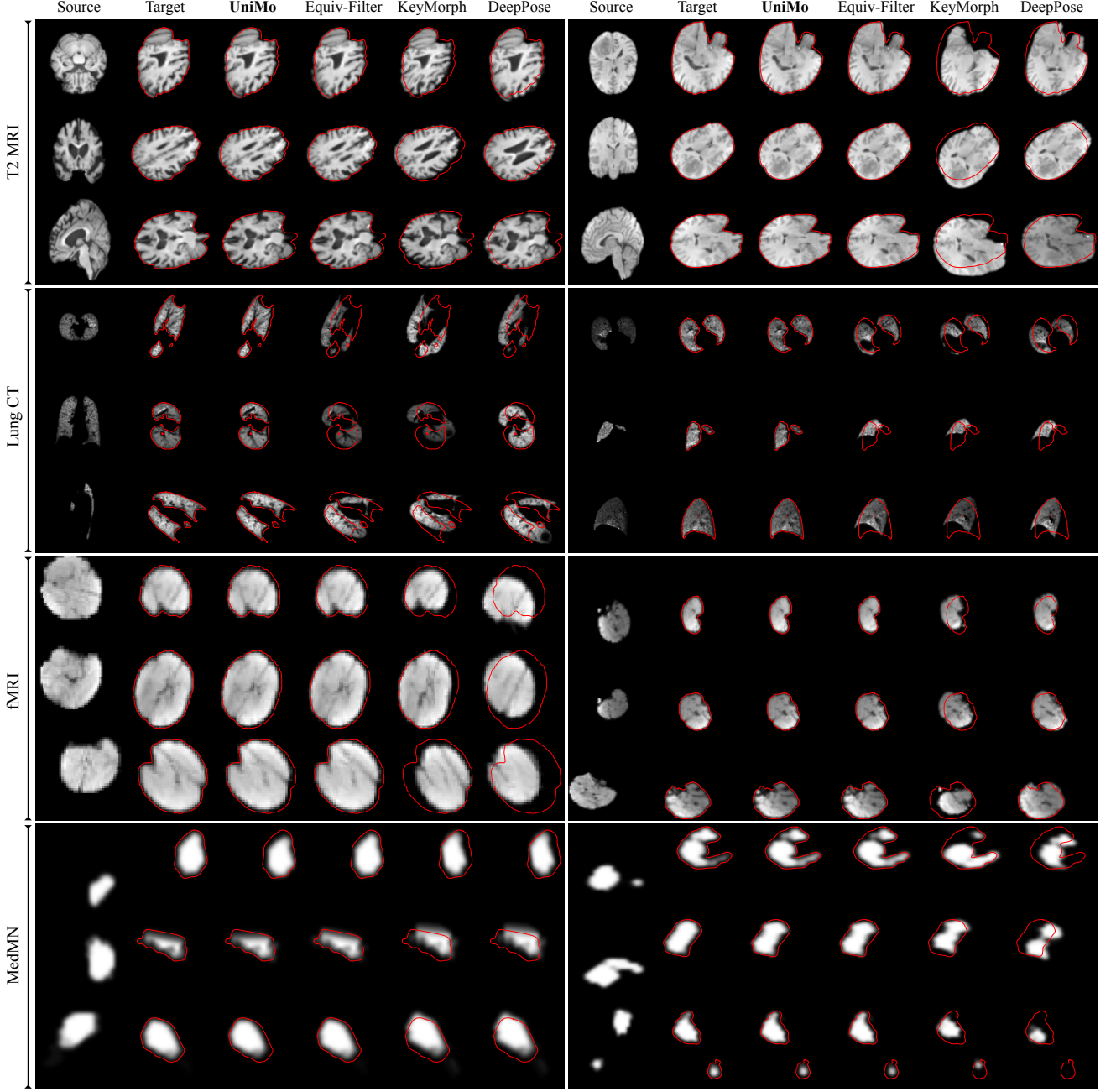


Fig. 5. Motion correction comparison across multiple image modalities for all models. The image modalities from top to bottom are: T1 MRI scans of brains containing lesions, lung CT scans, EPI scans of fetal brains, and the shapes of adrenal glands. The images from left to right are: source, target, and aligned images by UniMO, Equivariant Filter [17], KeyMorph [14], and DeepPose [11]. The aligned images are displayed with red contours for better visualization.

generalizability of UniMo across diverse imaging conditions.

## VI. DISCUSSION

Our approach builds on the extensive body of work in motion correction and tracking, combining the robustness of traditional techniques with the flexibility and efficiency of modern deep learning models. By integrating shape information and leveraging advanced neural network architectures, we provide a comprehensive solution that overcomes the limitations of existing methods, ensuring accurate and reliable motion correction. Fast inference allows its use in real-time motion estimation and correction. This advancement

represents a significant step forward in medical imaging, particularly in challenging domains such as fetal MRI, and paves the way to use advanced imaging to develop more effective diagnosis, prognosis, and therapeutic interventions.

UniMo is designed to robustly handle a broad spectrum of motion types commonly encountered in clinical imaging, including rigid transformations (e.g., head rotations [21], patient repositioning [64]), periodic non-rigid motion [65] (e.g., respiratory and cardiac motion), and gradual anatomical changes [66] (e.g., tumor growth, brain atrophy, or edema). By leveraging shape-aware priors, UniMo maintains registration accuracy even when intensity-based features are inconsistent

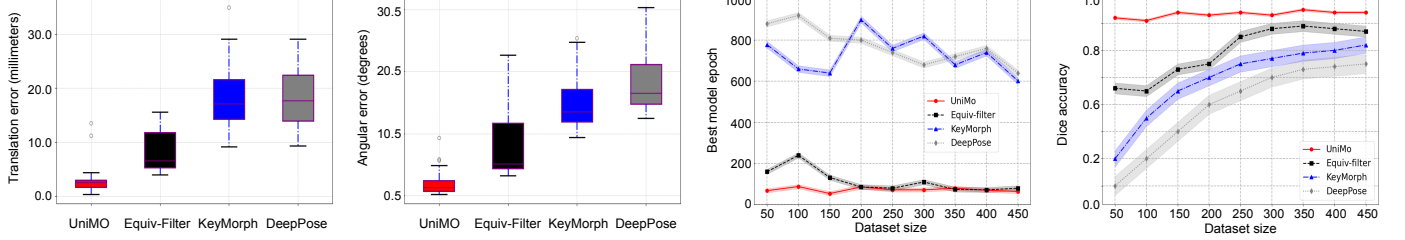


Fig. 6. From left to right: translational and angular errors of motion correction of four image modalities, epoch number of best model performance from training with varying training dataset size, and quantitative report of Dice accuracy with varying training dataset size.

or degraded. Clinically, this enables more reliable alignment for longitudinal studies [67] (e.g., monitoring neurodegeneration or treatment response), correction of motion artifacts in dynamic imaging [68] (e.g., abdominal or thoracic scans), and improved fusion across sessions or modalities. Robust performance for various motion types can support a range of applications spanning from longitudinal analysis to diagnosis, real-time interventions, and therapy planning.

## VII. CONCLUSION

In this paper, we introduced UniMo, a Universal Motion Correction framework as a framework that leverages deep neural networks to address the challenges of motion correction across various imaging datasets. By employing advanced neural network architectures with equivariant filters, UniMo overcomes the limitations of existing methods that require iterative retraining for each new image modality. Instead, UniMo achieves remarkable stability and adaptability through a single training phase on one modality, enabling effective application across multiple unseen modalities. UniMo excels by integrating hybrid knowledge from both shape and image data, significantly improving motion correction accuracy despite variations in image appearance. The inclusion of a geometric deformation augmenter enhances robustness by mitigating local geometric distortions and generating augmented data, thereby refining the training process. Experimental results across four distinct image datasets with various modalities demonstrate that UniMo outperforms current motion correction methods, representing a substantial advancement in medical imaging, particularly for complex image-guided motion correction applications such as real-time fetal head motion tracking. Looking ahead, several promising avenues for future work emerge. Firstly, exploring real-time applications and integrating UniMo with other imaging technologies, such as image segmentation, could enhance its utility in dynamic environments. Secondly, investigating advanced methods for selecting and utilizing different shape descriptors within UniMo may further boost joint learning performance and overall effectiveness.

## REFERENCES

- [1] M. Zaitsev, J. Maclarens, and M. Herbst, “Motion artifacts in mri: A complex problem with many partial solutions,” *Journal of Magnetic Resonance Imaging*, vol. 42, no. 4, pp. 887–901, 2015.
- [2] J. Maclarens, M. Herbst, O. Speck, and M. Zaitsev, “Prospective motion correction in brain imaging: a review,” *Magnetic resonance in medicine*, vol. 69, no. 3, pp. 621–636, 2013.
- [3] C. Malamatienou *et al.*, “Motion-compensation techniques in neonatal and fetal mr imaging,” *American Journal of Neuroradiology*, vol. 34, no. 6, pp. 1124–1136, 2013.
- [4] A. Z. Kyme and R. R. Fulton, “Motion estimation and correction in spect, pet and ct,” *Physics in Medicine & Biology*, vol. 66, no. 18, p. 18TR02, 2021.
- [5] J. M. Fitzpatrick, D. L. Hill, C. R. Maurer *et al.*, “Image registration,” *Handbook of medical imaging*, vol. 2, pp. 447–513, 2000.
- [6] N. White *et al.*, “Promo: real-time prospective motion correction in mri using image-based tracking,” *Magnetic Resonance in Medicine: An Official Journal of the International Society for Magnetic Resonance in Medicine*, vol. 63, no. 1, pp. 91–105, 2010.
- [7] E. Ferrante and N. Paragios, “Slice-to-volume medical image registration: A survey,” *Medical image analysis*, vol. 39, pp. 101–123, 2017.
- [8] A. Gholipour and N. Kehtarnavaz, “Biomedical image registration,” *Encyclopedia of Image Processing*, pp. 24–39, 2019.
- [9] Y. Sui, O. Afacan, A. Gholipour, and S. K. Warfield, “Slimm: Slice localization integrated mri monitoring,” *NeuroImage*, vol. 223, p. 117280, 2020.
- [10] S. Neves Silva *et al.*, “Real-time fetal brain tracking for functional fetal mri,” *Magnetic resonance in medicine*, vol. 90, no. 6, pp. 2306–2320, 2023.
- [11] S. S. M. Salehi, S. Khan, D. Erdogmus, and A. Gholipour, “Real-time deep pose estimation with geodesic loss for image-to-template rigid registration,” *IEEE transactions on medical imaging*, vol. 38, no. 2, pp. 470–481, 2018.
- [12] C. Calixto *et al.*, “Advances in fetal brain imaging,” *Magnetic Resonance Imaging Clinics*, vol. 32, no. 3, pp. 459–478, 2024.
- [13] V. Spieker *et al.*, “Deep learning for retrospective motion correction in mri: a comprehensive review,” *IEEE Transactions on Medical Imaging*, 2023.
- [14] M. Y. Evan, A. Q. Wang, A. V. Dalca, and M. R. Sabuncu, “Keymorph: Robust multi-modal affine registration via unsupervised keypoint detection,” in *International Conference on Medical Imaging with Deep Learning*. PMLR, 2022, pp. 1482–1503.
- [15] J. Wang, R. Faghahipirayesh, P. Golland, and A. Gholipour, “Spaer: Learning spatio-temporal equivariant representations for fetal brain motion tracking,” in *International Workshop on Preterm, Perinatal and Paediatric Image Analysis*. Springer, 2024, pp. 3–13.
- [16] J. Wang, R. Faghahipirayesh, D. Erdogmus, and A. Gholipour, “Joint motion estimation with geometric deformation correction for fetal echo planar images via deep learning,” in *Medical Imaging with Deep Learning*, 2024.
- [17] D. Moyer, E. Abaci Turk, P. E. Grant, W. M. Wells, and P. Golland, “Equivariant filters for efficient tracking in 3d imaging,” in *Medical Image Computing and Computer Assisted Intervention–MICCAI 2021: 24th International Conference, Strasbourg, France, September 27–October 1, 2021, Proceedings, Part IV 24*. Springer, 2021, pp. 193–202.
- [18] J. Xu, D. Moyer, P. E. Grant, P. Golland, J. E. Iglesias, and E. Adalsteinsson, “Svort: iterative transformer for slice-to-volume registration in fetal brain mri,” in *International Conference on Medical Image Computing and Computer-Assisted Intervention*. Springer, 2022, pp. 3–13.
- [19] M. W. Haskell *et al.*, “Network accelerated motion estimation and reduction (namer): convolutional neural network guided retrospective motion correction using a separable motion model,” *Magnetic resonance in medicine*, vol. 82, no. 4, pp. 1452–1461, 2019.
- [20] J. Schlemper, J. Caballero, J. V. Hajnal, A. N. Price, and D. Rueckert, “A deep cascade of convolutional neural networks for dynamic mr image reconstruction,” *IEEE transactions on Medical Imaging*, vol. 37, no. 2, pp. 491–503, 2017.

- [21] A. Singh, S. S. M. Salehi, and A. Gholipour, “Deep predictive motion tracking in magnetic resonance imaging: application to fetal imaging,” *IEEE transactions on medical imaging*, vol. 39, no. 11, pp. 3523–3534, 2020.
- [22] Q. Lyu *et al.*, “Cine cardiac mri motion artifact reduction using a recurrent neural network,” *IEEE Transactions on Medical Imaging*, vol. 40, no. 8, pp. 2170–2181, 2021.
- [23] J. Xu *et al.*, “Nesvor: implicit neural representation for slice-to-volume reconstruction in mri,” *IEEE transactions on medical imaging*, vol. 42, no. 6, pp. 1707–1719, 2023.
- [24] S. Chatterjee, A. Sciarra, M. Dünnwald, S. Oeltze-Jafra, A. Nürnberger, and O. Speck, “Retrospective motion correction of mr images using prior-assisted deep learning,” *arXiv preprint arXiv:2011.14134*, 2020.
- [25] M. A. Al-Masni, S. Lee, A. K. Al-Shamiri, S.-M. Gho, Y. H. Choi, and D.-H. Kim, “A knowledge interaction learning for multi-echo mri motion artifact correction towards better enhancement of swi,” *Computers in biology and medicine*, vol. 153, p. 106553, 2023.
- [26] E. Kuzmina, A. Razumov, O. Y. Rogov, E. Adalsteinsson, J. White, and D. V. Dylov, “Autofocusing+: noise-resilient motion correction in magnetic resonance imaging,” in *International Conference on Medical Image Computing and Computer-Assisted Intervention*. Springer, 2022, pp. 365–375.
- [27] J. Hossbach *et al.*, “Deep learning-based motion quantification from k-space for fast model-based magnetic resonance imaging motion correction,” *Medical physics*, vol. 50, no. 4, pp. 2148–2161, 2023.
- [28] H. Eichhorn *et al.*, “Physics-informed deep learning for motion-corrected reconstruction of quantitative brain mri,” in *MICCAI*, 2024.
- [29] N. M. Singh, J. E. Iglesias, E. Adalsteinsson, A. V. Dalca, and P. Golland, “Joint frequency and image space learning for mri reconstruction and analysis,” *The journal of machine learning for biomedical imaging*, vol. 2022, 2022.
- [30] L. Cui *et al.*, “Motion artifact reduction for magnetic resonance imaging with deep learning and k-space analysis,” *PloS one*, vol. 18, no. 1, p. e0278668, 2023.
- [31] G. Seegoolam, J. Schlemper, C. Qin, A. Price, J. Hajnal, and D. Rueckert, “Exploiting motion for deep learning reconstruction of extremely undersampled dynamic mri,” in *International Conference on Medical Image Computing and Computer-Assisted Intervention*. Springer, 2019, pp. 704–712.
- [32] H. Qi *et al.*, “End-to-end deep learning nonrigid motion-corrected reconstruction for highly accelerated free-breathing coronary mra,” *Magnetic Resonance in Medicine*, vol. 86, no. 4, pp. 1983–1996, 2021.
- [33] W. Huang, H. B. Li, J. Pan, G. Cruz, D. Rueckert, and K. Hammernik, “Neural implicit k-space for binning-free non-cartesian cardiac mr imaging,” in *International Conference on Information Processing in Medical Imaging*. Springer, 2023, pp. 548–560.
- [34] V. Spieker *et al.*, “Iconik: Generating respiratory-resolved abdominal mr reconstructions using neural implicit representations in k-space,” in *MICCAI*. Springer, 2023, pp. 183–192.
- [35] S. Harput *et al.*, “Two-stage motion correction for super-resolution ultrasound imaging in human lower limb,” *IEEE transactions on ultrasonics, ferroelectrics, and frequency control*, vol. 65, no. 5, pp. 803–814, 2018.
- [36] R. Prevost *et al.*, “3d freehand ultrasound without external tracking using deep learning,” *Medical image analysis*, vol. 48, pp. 187–202, 2018.
- [37] L. Shi *et al.*, “Automatic inter-frame patient motion correction for dynamic cardiac pet using deep learning,” *IEEE transactions on medical imaging*, vol. 40, no. 12, pp. 3293–3304, 2021.
- [38] T. Li, M. Zhang, W. Qi, E. Asma, and J. Qi, “Deep learning based joint pet image reconstruction and motion estimation,” *IEEE transactions on medical imaging*, vol. 41, no. 5, pp. 1230–1241, 2021.
- [39] B. Billot *et al.*, “Se (3)-equivariant and noise-invariant 3d motion tracking in medical images,” *arXiv preprint arXiv:2312.13534*, 2023.
- [40] A. Q. Wang, M. Y. Evan, A. V. Dalca, and M. R. Sabuncu, “A robust and interpretable deep learning framework for multi-modal registration via keypoints,” *Medical Image Analysis*, vol. 90, p. 102962, 2023.
- [41] J. Wang, J. Xing, J. Druzgal, W. M. Wells III, and M. Zhang, “Metamorph: Learning metamorphic image transformation with appearance changes,” in *International Conference on Information Processing in Medical Imaging*. Springer, 2023, pp. 576–587.
- [42] A. Q. Wang, R. Saluja, H. Kim, X. He, A. Dalca, and M. R. Sabuncu, “Brainmorph: A foundational keypoint model for robust and flexible brain mri registration,” *arXiv preprint arXiv:2405.14019*, 2024.
- [43] M. F. Beg, M. I. Miller, A. Trouvé, and L. Younes, “Computing large deformation metric mappings via geodesic flows of diffeomorphisms,” *International journal of computer vision*, vol. 61, pp. 139–157, 2005.
- [44] B. B. Avants, C. L. Epstein, M. Grossman, and J. C. Gee, “Symmetric diffeomorphic image registration with cross-correlation: evaluating automated labeling of elderly and neurodegenerative brain,” *Medical image analysis*, vol. 12, no. 1, pp. 26–41, 2008.
- [45] W. M. Wells III, P. Viola, H. Atsumi, S. Nakajima, and R. Kikinis, “Multi-modal volume registration by maximization of mutual information,” *Medical image analysis*, vol. 1, no. 1, pp. 35–51, 1996.
- [46] V. I. Arnol'd, “Sur la géométrie différentielle des groupes de Lie de dimension infinie et ses applications à l'hydrodynamique des fluides parfaits,” *Ann. Inst. Fourier*, vol. 16, pp. 319–361, 1966.
- [47] M. I. Miller, A. Trouvé, and L. Younes, “Geodesic shooting for computational anatomy,” *Journal of mathematical imaging and vision*, vol. 24, no. 2, pp. 209–228, 2006.
- [48] M. Zhang and P. T. Fletcher, “Fast diffeomorphic image registration via fourier-approximated lie algebras,” *International Journal of Computer Vision*, vol. 127, no. 1, pp. 61–73, 2019.
- [49] D. Vranic and D. Saupe, “3d shape descriptor based on 3d fourier transform,” 2001.
- [50] A. Khotanzad and Y. H. Hong, “Invariant image recognition by zernike moments,” *IEEE Transactions on pattern analysis and machine intelligence*, vol. 12, no. 5, pp. 489–497, 1990.
- [51] Z. Zhong *et al.*, “Slerpface: Face template protection via spherical linear interpolation,” *arXiv preprint arXiv:2407.03043*, 2024.
- [52] Y. K. Jang, D. Huynh, A. Shah, W.-K. Chen, and S.-N. Lim, “Spherical linear interpolation and text-anchoring for zero-shot composed image retrieval,” *arXiv preprint arXiv:2405.00571*, 2024.
- [53] J. Li, X. Su, X. Ma, and G. Gao, “Quatse: Spherical linear interpolation of quaternion for knowledge graph embeddings,” in *CCF International Conference on Natural Language Processing and Chinese Computing*. Springer, 2022, pp. 209–220.
- [54] G. Balakrishnan, A. Zhao, M. R. Sabuncu, J. Guttag, and A. V. Dalca, “Voxelmorph: a learning framework for deformable medical image registration,” *IEEE transactions on medical imaging*, vol. 38, no. 8, pp. 1788–1800, 2019.
- [55] J. Chen, E. C. Frey, Y. He, W. P. Segars, Y. Li, and Y. Du, “Transmorph: Transformer for unsupervised medical image registration,” *Medical image analysis*, vol. 82, p. 102615, 2022.
- [56] B. Kim, I. Han, and J. C. Ye, “Diffusemorph: Unsupervised deformable image registration using diffusion model,” in *European conference on computer vision*. Springer, 2022, pp. 347–364.
- [57] J. Nocedal and S. J. Wright, *Numerical optimization*. Springer, 1999.
- [58] R. Faghihiparayesh, D. Karimi, D. Erdoğmuş, and A. Gholipour, “Fetalbet: Brain extraction tool for fetal mri,” *IEEE Open Journal of Engineering in Medicine and Biology*, 2024.
- [59] J. Yang *et al.*, “Autosegmentation for thoracic radiation treatment planning: a grand challenge at aapm 2017,” *Medical physics*, vol. 45, no. 10, pp. 4568–4581, 2018.
- [60] J. Yang, R. Shi, and B. Ni, “Medmnist classification decathlon: A lightweight automb benchmark for medical image analysis,” in *2021 IEEE 18th International Symposium on Biomedical Imaging (ISBI)*. IEEE, 2021, pp. 191–195.
- [61] J. Yang *et al.*, “Medmnist v2-a large-scale lightweight benchmark for 2d and 3d biomedical image classification,” *Scientific Data*, vol. 10, no. 1, p. 41, 2023.
- [62] U. Baid *et al.*, “The rsna-asnr-miccai brats 2021 benchmark on brain tumor segmentation and radiogenomic classification,” *arXiv preprint arXiv:2107.02314*, 2021.
- [63] B. H. Menze *et al.*, “The multimodal brain tumor image segmentation benchmark (brats),” *IEEE transactions on medical imaging*, vol. 34, no. 10, pp. 1993–2024, 2014.
- [64] J. Wasza, S. Bauer, and J. Hornegger, “Real-time motion compensated patient positioning and non-rigid deformation estimation using 4-d shape priors,” in *International Conference on Medical Image Computing and Computer-Assisted Intervention*. Springer, 2012, pp. 576–583.
- [65] H. Qi *et al.*, “Non-rigid respiratory motion estimation of whole-heart coronary mr images using unsupervised deep learning,” *IEEE Transactions on Medical Imaging*, vol. 40, no. 1, pp. 444–454, 2020.
- [66] Y. Rong *et al.*, “Rigid and deformable image registration for radiation therapy: a self-study evaluation guide for nrg oncology clinical trial participation,” *Practical radiation oncology*, vol. 11, no. 4, pp. 282–298, 2021.
- [67] J. Lv *et al.*, “Joint progressive and coarse-to-fine registration of brain mri via deformation field integration and non-rigid feature fusion,” *IEEE Transactions on Medical Imaging*, vol. 41, no. 10, pp. 2788–2802, 2022.
- [68] S. Kurugol *et al.*, “Motion-robust parameter estimation in abdominal diffusion-weighted mri by simultaneous image registration and model estimation,” *Medical image analysis*, vol. 39, pp. 124–132, 2017.